Journal of Ceramic Processing Research. Vol. 13, No. 5, pp. 651~656 (2012)

JOURNAL OF
Ceramic Processing Research

Combustion synthesis of nanocrystalline Co and Al co-doped ZnO ($Zn_{1-x-y}Co_xAl_yO$) and its powder characteristics

R. Siddheswaran[a,*], R.V. Mangalaraja[a,*], Ricardo E. Avila[b], D. Manikandan[a], Marta Lopez[a], C. Esther Jeyanthi[c], S. Ananthakumar[d]

[a]*Advanced Ceramics and Nanotechnology Laboratory, Department of Materials Engineering, University of Concepcion, Concepcion, Chile*

[b]*Personal Dosimetry Section, Chilean Commission of Nuclear Energy, Santiago, Chile*

[c]*Research and Development Centre, Bharathiar University, Coimbatore - 641 046, India*

[d]*Materials and Mineral Division, National Institute for Interdisciplinary Science and Technology, CSIR, Trivandrum-695019, Kerala, India*

Co, Al **co-doped zinc oxide [$Zn_{1-x-y}Co_xAl_yO$; x = 0.04, 0.03, 0.02; y = 0.01, 0.02, 0.03] nanoparticles were synthesized by a citrate assisted combustion method at 500 °C for various doping levels using zinc, cobalt and aluminum nitrates as precursors. The synthesized oxide nanopowders of different compositions were calcined at 600, 700 and 800 °C for 2 h. The synthesized $Zn_{1-x-y}Co_xAl_yO$ nanocrystals were characterized for their thermal, structural, and morphological features. The structural studies resulting in doping-independent crystallite sizes and the thermal analysis confirm the execution of complete combustion. The average particle size of ZnO nanocrystals decreases due to the tension caused by *Co* and *Al* dopants in the zincite structure and the ionic size differences. The as-prepared nanoparticles with an average particle size in the range of 10-20 and 20-30 nm were observed for doped and undoped ZnO, respectively.**

Key words: Combustion synthesis, ZnO, Nanoparticles, Co-dopants.
PACS: 61.46.Hk, 63.22.Kn, 65.80.-g, 68.37.Hk, 68.37.Lp, 75.75.Cd; 81.07.Bc.

Introduction

An existing possibility to utilize both the charge and spin characters of an electron to develop spintronic devices such as field effect transistors (FETs) and light emitting transistors (LEDs) has led to extensive search for materials in which semiconducting properties can be integrated with magnetic properties. These materials are categorized as dilute magnetic semiconductors (DMSs) which are fabricated by introducing small fractions of transition metals (TMs) into host (non magnetic) semiconductors, e.g., III-V and II-VI compounds [1-4]. The essential requirement for achieving practical spintronic devices is efficient electrical injection of spin-polarized charge carriers. The material should be capable of transporting the carriers with high transmission efficiency in the host semiconductor. These key aspects of spin injection, spin-dependent transport manipulation and detection form the basis of current research and future technology of spintronics. The low power consumption of these devices has the advantage of resulting in high packing densities for memory elements. Thus from the industrial application point-of-view, it is important for a DMS to be an efficient conductor and ferromagnetic at room temperature [5-10]. Many researchers made theoretical predictions for room temperature ferromagnetism in heavily doped p-type ZnO alloy [11-13]. Since p-type ZnO is difficult to fabricate, much work has been done on n-type ZnO with various transition metal dopants. *Co* is chosen since its ionic radius matches with a Zn^{2+} ion resulting in high solubility. *Al* is a good co-dopant as it is an adequate electron donor and has no '*d*' electrons to interfere with magnetic ordering. Early experimental reports provide some mixed and even contradicting results. In one of the studies of doping various TMs into ZnO by Ueda et al. [14] confirmed a highly conducting n-type *Co* doped ZnO displayed room temperature ferromagnetism. Other studies found that the ferromagnetism is extrinsic in nature and arises from nanoclusters and secondary magnetic phases [15-18]. Hence, it is essential to study the $Zn_{1-x-y}Co_xAl_yO$ system in detail to understand its structural, electrical and optical properties as they play an important role in determining and promoting ferromagnetism.

Various methods have been used to synthesize pure or TM doped ZnO nanomaterials [19-22]. Finding a new methodology to synthesize uniform nano-sized ZnO particles is of great importance for both fundamental

*Corresponding author:
Tel : +56-41-2203664
Fax: +56-41-2203391
E-mail: rsiddhes@yahoo.com ; mangal@udec.cl

studies and practical applications, and thus different methods such as thermal decomposition; chemical vapor deposition, sol-gel, spray pyrolysis, solution combustion and precipitation have been developed. The combustion method has been found to be unique to obtain fine particles of high surface area [23, 24]. This is a low temperature technique that offers an exothermic redox reaction to produce oxides. A combustion reaction can be influenced by various processing parameters such as the type of fuel, the fuel-to-oxidizer ratio (F/O), the water content of the precursor mixture and the ignition temperature. Many authors have reported the combustion synthesis of ZnO [25-27]. In the present study, pure and transition metal doped ZnO [$Zn_{1-x-y}Co_xAl_yO$] have been synthesized by combustion. The powder characteristics of the $Zn_{1-x-y}Co_xAl_yO$ nanocrystals were also studied and reported.

Experimental

Stoichiometric amounts of highly purified $Zn(NO_3)_2.6H_2O$ (99.0%), $Co(NO_3)_2.6H_2O$ (99.99%) and $Al(NO_3)_3.9H_2O$ (99.99%) metal nitrates were dissolved together in a minimum amount of distilled water to get a clear and viscous precursor solution. The required amount of citric acid was mixed with the nitrates solution. Citric acid has a double function; being the metal ion's complexant as well as the fuel. The citric acid/metal nitrates ratio (C/M) was calculated from the basic principle of propellant chemistry [28]. The mixture of solutions was stirred mechanically for 2 h at 60 °C until a sticky gel was obtained. After making the clear homogeneous precursor gel, the reaction mixture was transferred into an alumina crucible and it was kept inside a preheated furnace at a temperature of 500 °C. Once the reaction mixture reached the point of spontaneous combustion, it started burning vigorously. During the combustion reactions, gaseous volatile molecules such as N_2, CO_2, H_2O and other forms of gaseous products were released, in the form of brown fumes. Finally, a porous solid foam of nanoparticles was obtained within 10 minutes. The assumed combustion reactions involved among metal nitrates and fuel with different stoichiometric ratios are given in table 1. The as-combusted foams were collected and converted to powders by simple grinding. The same process was repeated for different dopant ratios of *Co* and *Al*. The as-prepared powders of different compositions (x, y) weight percent of (0.04, 0.01), (0.03, 0.02) and (0.02, 0.03) were calcined at 600, 700 and 800 °C for 2 h (at a heating rate of 5 K/minute).

The as-combusted ZnO and $Zn_{1-x-y}Co_xAl_yO$ powders were characterized by thermogravimetry (TGA) and differential thermal analysis (DTA) using a Netzsch-STA 409 PC/PG. To study the crystalline structure, a Siemens D5000 diffractometer was used with Cu-$K\alpha$ radiation, operating at 40 kV, 20 mA, with a graphite monochromator. The 2θ step size was 0.02 ° with the integration time of 1s per step, over the 2θ scan range of 5 to 75 °. The surface area and equivalent spherical diameter of the particles have been determined from BET [29] theory by nitrogen adsorption/desorption measurements at 77 K, using a Micromeritics-Gemini 2360 instrument. All the samples were pre-treated in vacuum at 250 °C for 1.5 h prior to the measurements. The surface morphology and the presence of elements in the samples were examined using a scanning electron microscope (SEM-JEOL 6460 LV) fitted with an energy dispersive X-ray spectrometer. The morphology and microstructure of as-synthesized and calcined nanoparticles were investigated using a transmission electron microscope (TEM-JEOL JEM 2000 EX) equipped with EDS. The samples for TEM were prepared by dispersing the samples in 50-50% water-ethanol with ultrasonic agitation and the dispersed particles were dropped on copper grids covered by an amorphous carbon film.

Results and discussion

TGA/DTA responses recorded at a constant heating rate of 2 K/minute in a *He* atmosphere are shown in fig. 1. It was found that the thermograms are almost similar for all the samples. In the TGA trace, no prominent weight losses were observed, which confirms the execution of complete combustion at 500 °C leaving no organic residues. The endothermic DTA trace above 400 °C which can be associated to the crystal phase formation temperature of metal oxides. Subsequently, after the saturated crystallization at

Table 1. Assumed chemical reaction during the combustion on various ratios of dopants and fuel

Chemical reactions			
$0.95[Zn(NO_3)_2.6H_2O] + 0.04[Co(NO_3)_2.6H_2O] + 0.01[Al(NO_3)_3.9H_2O] + 0.5583[CH_2COOHCOHCOOHCH_2COOH]$	→	$Zn_{0.95}Co_{0.04}Al_{0.01}O$ + Molecular gases	↑
$0.95[Zn(NO_3)_2.6H_2O] + 0.03[Co(NO_3)_2.6H_2O] + 0.02[Al(NO_3)_3.9H_2O] + 0.5611[CH_2COOHCOHCOOHCH_2COOH]$	→	$Zn_{0.95}Co_{0.03}Al_{0.02}O$ + Molecular gases	↑
$0.95[Zn(NO_3)_2.6H_2O] + 0.02[Co(NO_3)_2.6H_2O] + 0.03[Al(NO_3)_3.9H_2O] + 0.5639[CH_2COOHCOHCOOHCH_2COOH]$	→	$Zn_{0.95}Co_{0.02}Al_{0.03}O$ + Molecular gases	↑
$Zn(NO_3)_2.6H_2O + 0.5555[CH_2COOHCOHCOOHCH_2COOH]$	→	ZnO + Molecular gases	↑

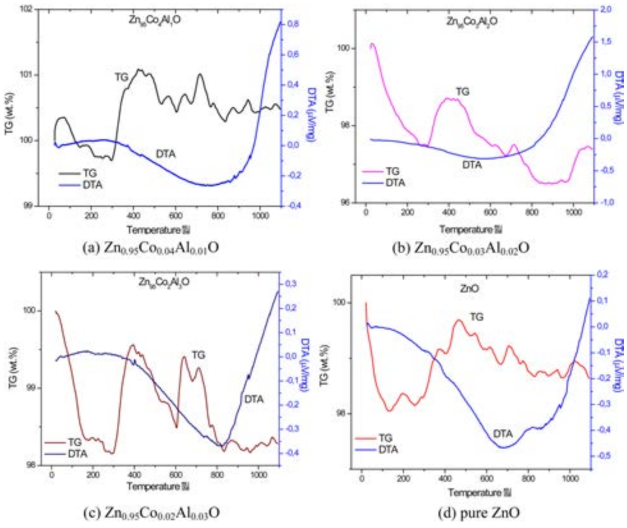

Fig. 1. TG/DTA traces of pure ZnO and $Zn_{1-x-y}Co_xAl_yO$

800 °C the system evolves energy which is shown as an exothermic trace. The ZnO and $Zn_{1-x-y}Co_xAl_yO$ complex system shows the crystalline phase changes only from 500-800 °C.

X-ray diffraction measurements carried out on a series of $Zn_{1-x-y}Co_xAl_yO$ complexes for different calcination temperatures are shown in fig. 2. The diffraction patterns indicate that there are no traces of cobalt and aluminum oxides and any binary zinc-cobalt or zinc-aluminum, and ternary zinc-cobalt-aluminum phases have been observed. Hence it confirms the substitution of *Co* and *Al* dopants into ZnO and the formation of a singular phase $Zn_{1-x-y}Co_xAl_yO$. It is also evident from that the as-prepared and calcined powders of all the dopant combinations have the same crystalline hexagonal wurtzite structure. The mean crystallite size (t) of the nanoparticles were calculated from the XRD line-broadening measurement using the Debye-Scherrer's equation [30]:

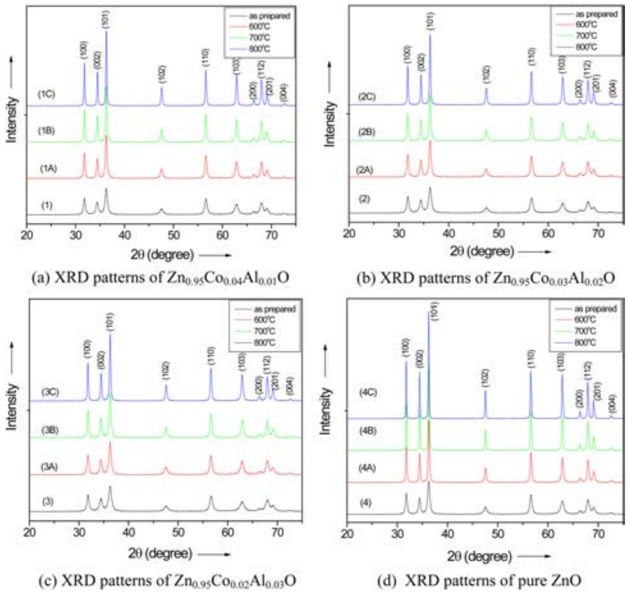

Fig. 2. X-ray diffraction patterns of pure ZnO and $Zn_{1-x-y}Co_xAl_yO$

$$\tau = \frac{K\lambda}{\Delta\beta \cdot cos(\theta)} \qquad (1)$$

where, the shape factor, *K*, is given the value 0.9, assuming mostly Gaussian diffraction peaks, λ is the X-ray wavelength, $\Delta\beta = \sqrt{\beta_s^2 - \beta_i^2}$, β_s and β_i being the FWHM of the sample and of the instrument, respectively. The crystallite size range of as-combusted powders was found to be 25-27 nm. Similarly, the particles size range of the calcined powders at 600, 700 and 800 °C were calculated in the range of 32-41 nm, 40-51 nm and 48-61 nm, respectively as shown in table 2. The calculated values are consistent with the measured values from transmission electron microscopy (TEM). The calcined powders induce highly narrow diffraction

Table 2. Particles size from X-ray diffraction patterns using Scherrer's equation

Composition/ Calcination temp.	Particles size (nm)			
	Synthesized	Calcined at 600 °C	Calcined at 700 °C	Calcined at 800 °C
$Zn_{0.95}Co_{0.04}Al_{0.01}O$	26	33	41	49
$Zn_{0.95}Co_{0.03}Al_{0.02}O$	24	35	42	49
$Zn_{0.95}Co_{0.02}Al_{0.03}O$	24	33	37	49
ZnO	27	41	51	60

Table 3. BET surface area and equivalent diameters of the nanoparticles for various compositions

MATE-RIAL	$Zn_{0.95}Co_{0.04}Al_{0.01}O$				$Zn_{0.95}Co_{0.03}Al_{0.02}O$				$Zn_{0.95}Co_{0.02}Al_{0.03}O$				ZnO			
TEMP.	AP*	600 °C	700 °C	800 °C	AP*	600 °C	700 °C	800 °C	AP*	600 °C	700 °C	800 °C	AP*	600 °C	700 °C	800 °C
S_{BET} (m^2/g)	37.1	25.9	19.5	16.6	36.9	27.2	20.3	15.1	35.6	26.9	18.4	14.2	23.6	19.8	14.7	11.0
D_{BET} (nm)	29	41	55	64	29	39	53	71	30	40	59	76	45	54	73	97

*AP – as-prepared

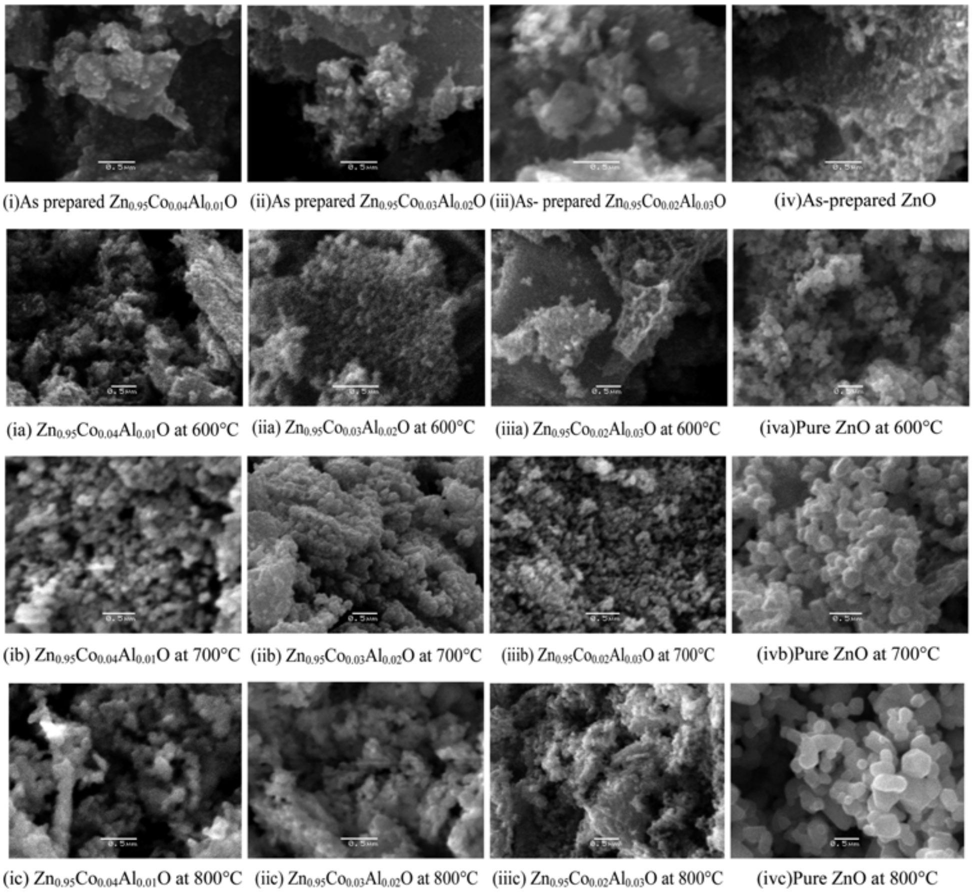

Fig. 3. SEM micrographs of pure ZnO and $Zn_{1-x-y}Co_xAl_yO$

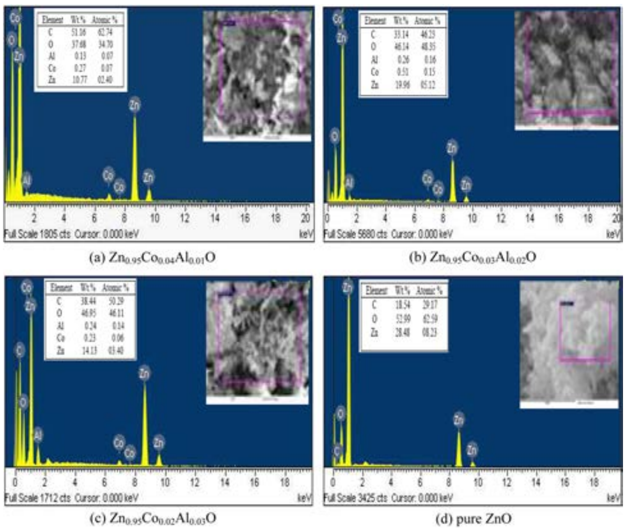

Fig. 4. SEM attached EDS spectra of the pure ZnO and $Zn_{1-x-y}Co_xAl_yO$

peaks compared to the as-combusted powders, supporting the crystal growth process during calcination up to 800 °C.

The high surface area in the as-combusted powder is due to the presence of highly porous agglomerates and clustering of amorphous nanoparticles. Whereas, the surface area decreases considerably for the calcined samples this causes the increase in crystallinity. The equivalent diameter of the particles (D_{BET}) were calculated from BET data according to the equation $D_{BET} = 6/(\rho_{th}S_{BET})$, where, S_{BET} is the measured surface area and ρ_{th} is the theoretical density of the compound [31]. Table 3 displays a comparison of BET specific surface areas of the pure and co-doped (Co, Al) ZnO. The equivalent diameters of doped ZnO were lower than those of the pure samples and they are directly proportional to the calcination temperature.

The morphologies of the as-prepared and calcined samples at different temperatures are shown by the SEM micrographs (Fig. 3). Since the dopant concentrations are very low, the morphologies of the powders are almost similar but the particle size increases with the calcination temperature. The large particles are composed of small crystallites and show particle aggregates of spherical shapes. The energy dispersive X-ray spectra (EDS) in fig. 4 performed on the nanoparticles reports the presence of *Zn, Co, Al* and *O* elements. The *C* and *Au* peaks stems from the conductive surface of samples sprayed with carbon and gold. Transmission electron micrographs shown in fig. 5 show the nanoparticles are uniform in size and shape. The particle size increases with the calcination temperature and the average particle size of the *Co* and *Al* doped ZnO nanopowders are smaller than those of the pure ZnO. This is due to the tension caused by the

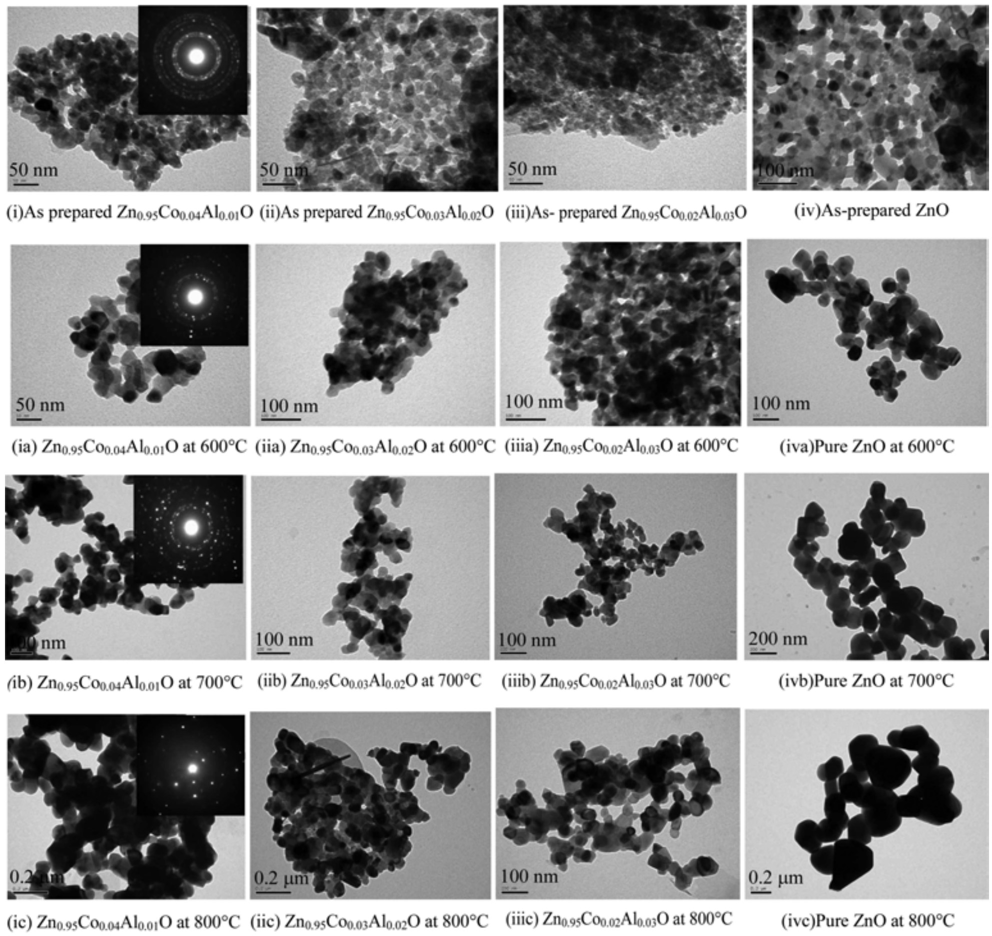

Fig. 5. TEM micrographs of the hexagonal nanocrystalline pure ZnO and $Zn_{1-x-y}Co_xAl_yO$

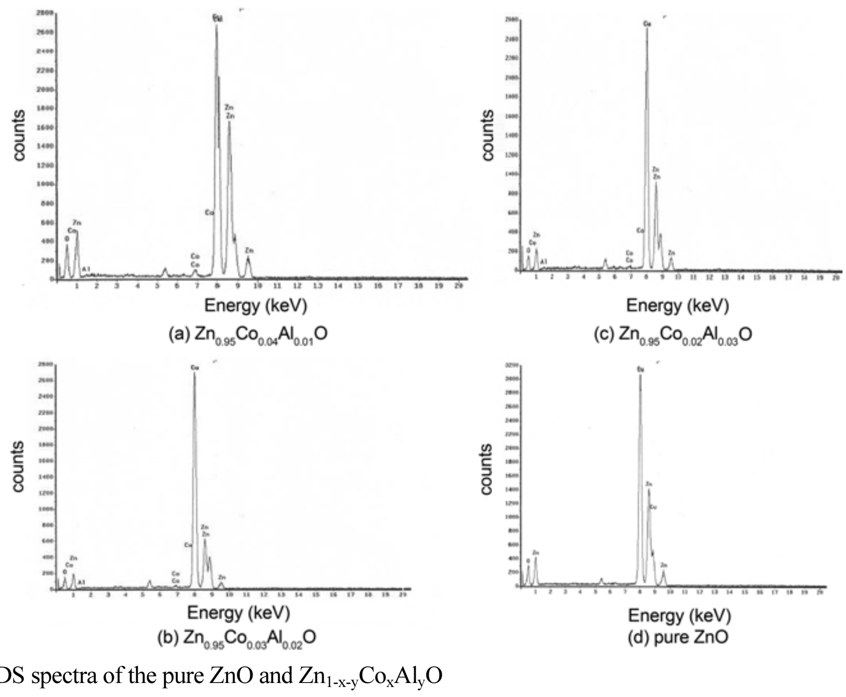

Fig. 6. TEM attached EDS spectra of the pure ZnO and $Zn_{1-x-y}Co_xAl_yO$

dopant impurities in the zincite structure and their ionic size difference to that of Zn^{2+}. Also the dopant impurities affect the growth of nanoparticles during the combustion since the dopants act as catalysts for size reduction. The as-prepared nanoparticles with an average particle size in the range of 10-20 and 20-

30 nm were observed for doped and undoped ZnO, respectively. The high crystallinity of the powder leads to its corresponding well-pronounced Debye–Scherrer diffraction rings in the selected area electron diffraction (SAED) pattern attached with the TEM micrographs. The calculated values from XRD provide volume-weighted average crystalline sizes in the range of 25-60 nm, which is in good agreement with the particle size observed in the TEM. From the TEM attached EDS spectra (Fig. 6), peaks ascribed to *Zn, Co, Al* and *O* were detected for the prepared nanoparticles and this confirms the presence of elements in the composition. Peaks corresponding to *Cu* and *C* were also detected from the carbon coated copper grid.

Conclusions

Fine nanoparticles of pure and *Co, Al* co-doped ZnO [$Zn_{1-x-y}Co_xAl_yO$] were successfully synthesized by a combustion reaction. The thermal analysis confirms that there are no prominent weight losses during the heating due to the execution of complete combustion reaction synthesis leaving no organic residues. It was found that no traces of dopant phases have been observed in $Zn_{1-x-y}Co_x Al_yO$ composite although the EDS shows the presence of *Co* and *Al*, which confirms the substitution of *Co, Al* are doped into ZnO and the formation of a $Zn_{1-x-y}Co_xAl_yO$ singular phase. Hence, it proves that the as-prepared and calcined powders of all the dopant combinations have the same crystalline hexagonal wurtzite structure. The particle size increases with the calcination temperature and the average particle size of the *Co* and *Al* doped ZnO nanopowders are smaller than the pure ZnO. The surface morphology, shape and size of the nanoparticles were characterized by scanning and transmission electron microscopy. The energy dispersive X-ray spectroscopic study confirms the presence of elements in the composition.

Acknowledgements

The authors would like to thank FONDECYT, Govt. of Chile (Project No. : 3110026) and Direction of investigation, University of Concepcion, Chile for the financial assistance and supports.

References

1. H. Munekata, H. Ohno, S. Von Molnar, Armin Segmüller, L.L. Chang, and L. Esaki, Phys. Rev. Lett. 63 [17] (1989) 1849-1852.
2. Yu. Uspenskii, E. Kulatov, A. Titov, H. Mariette, J. Cibert, K. Motizukie, H. Nakayama, H. Ohtag, J. Magn. Magn. Mater. 300 [1] (2006) 140-143.
3. Y.O. Ciftci, X.F. Wang, P. Vasilopoulos, Physica E: Low-dimensional Systems and Nanostructures 30 [1-2] (2005) 74-80.
4. K. Kayanuma, S. Shirotori, Z.H. Chen, T. Tomita, A. Murayama, Y. Oka, Physica B: Condensed Matter 340-342 [31] (2003) 882-885.
5. J.M. Kikkawa, I.P. Smorchkova, N. Samarth, and D.D. Awschalom, Science 277 (1989) 1284-1287.
6. H. Ohno, Science 281 (1989) 951-956.
7. R. Fiederling, M. Keim, G. Reuscher, W. Ossau, G. Schmidt, A. Waag, and L.W. Molenkamp, Nature 402 (1999) 787-790.
8. B.T. Jonker, Y.D. Park, B.R. Bennett, H.D. Cheong, G. Kioseoglou, and A. Petrou, Phys. Rev. B 62 (2000) 8180-8183.
9. T. Dietl, H. Ohno, and F. Matsukura, Phys. Rev. B 63 (2001) 195205-1.
10. T. Slupinski, H. Munekata, and A. Oiwa, Extended Abstracts, 7th Symp. On the Physics and Application of Spin-Related Phenomena in Semiconductors, Yokohama, Japan, Dec. 17-8 (2001) 52.
11. O. Mounkachi, A. Benyoussef, A. El Kenz, E.H. Saidi, E.K. Hlil, Physica A: Statistical Mechanics and its Applications 388 [17] 1 (2009) 3433-3441.
12. Lanli Chen, Zhihua Xiong, Qixin Wan, Dongmei Li, Optical Materials 32 [9] (2010) 1216-1222.
13. In Soo Kim, Eun-Kyung Jeong, Do Yun Kim, Manoj Kumar, Se-Young Choi, Appl. Surf. Sci. 255 [7] 15 (2009) 4011-4014.
14. K. Ueda, H. Tabata, T. Kawai, Appl. Phys. Lett. 79 (2001) 988-990.
15. Y. Kalyana Lakshmi, K. Srinivas, B. Sreedhar, M. Manivel Raja, M. Vithal, P. Venugopal Reddy, Mater. Chem. and Phys. 113 [2-3] (2009) 749-755.
16. Liqiang Zhang, Zhizhen Ye, Bin Lu, Jianguo Lu,Haiping He, Yinzhu Zhang, Liping Zhu, Jie Jiang, Kewei Wu, Bo He, Superlattices and Microstructures, 50 [3] (2011) 261-268.
17. In-Bo Shim, Chul Sung Kim, J. Magn. Magn. Mater., 272-276, Supplement (2004) E1571-E1572.
18. Kanwal Preet Bhatti, Sujeet Chaudhary, Dinesh K. Pandya, Subhash C. Kashyap, Solid State Communications 140 [1] (2006) 23-27.
19. B.Q. Wang, P.W. Wang, X.J. Zhang, X.Z. Zhang, H.G. Fu, L.Q. Jing, D.P. Yu, Chin. J. Inorg. Chem. 23 [8] (2007) 1365-1368.
20. Chengbin Jing, Yingjing Jiang, Wei Bai, Junhao Chu, Aiyun Liu, J. Magn. Magn. Mater., 322 [16] (2010) 2395-2400.
21. Xingyan Xu, Chuanbao Cao, J. Alloys Compd. 501 [2] (2010) 265-268.
22. Yingjing Jiang, Wei Wang, Chengbin Jing, Chunyue Cao, Junhao Chu, Mater. Sci. Engg.: B176 [16] (2011) 1301-1306.
23. R.V. Mangalaraja, S. Thomas Lee, S. Ananthakumar, P. Manohar, Carlos P. Camurri, Mater. Sci. Engg.: A 476 [1-2] (2008) 234-239.
24. R.V. Mangalaraja, S. Ananthakumar, M. Paulraj, H. Pesenti, Marta López, Carlos P. Camurri, Loreto A. Barcos, Ricardo E. Avila, J. Alloys Compd. 510 [1] (2012) 134-140.
25. C.C. Hwang, T.Y. Wu, J. Mater. Sci. 39 (2004) 6111-6115.
26. Y.N. Zhao, M.S. Cao, J.G. Li, Y.J. Chen, J. Mater. Sci. 41 (2006) 2243-2248.
27. Sousan Rasouli, Shirin Jebeli Moeen, J. Alloys Compd. 509 [5] (2011) 1915-1919.
28. S. Ekambaram, K.C. Patil, J. Mater. Chem. 5 [6] (1995) 905-908.
29. S. Brunauer, P.H. Emmett, and E. Teller, J. Am. Chem. Soc. 60 (1938) 309-319.
30. P. Scherrer, Göttinger Nachrichten Gesell. 2 (1918) 1-98.
31. R. Doshi, C.B. Alock, J.J. Carberry, Catal. Lett. 18 [4] (1993) 337-343.